ACS APPLIED MATERIALS & INTERFACES

Research Article

www.acsami.org

MicroRNA Functionalized Microporous Titanium Oxide Surface by Lyophilization with Enhanced Osteogenic Activity

Kaimin Wu,[†,∥] Wen Song,[†,∥] Lingzhou Zhao,[*,‡] Mengyuan Liu,[†] Jun Yan,[†] Morten Østergaard Andersen,[§] Jørgen Kjems,[§] Shan Gao,[§,⊥] and Yumei Zhang[*,†]

[†]Department of Prosthetic Dentistry and [‡]Department of Periodontology and Oral Medicine, School of Stomatology, The Fourth Military Medical University, No. 145 West Changle Road, Xi'an 710032, China

[§]The Interdisciplinary Nanoscience Center (iNANO) and Department of Molecular Biology and Genetics, Aarhus University, 8000 Aarhus C, Denmark

ABSTRACT: Developing biomedical titanium (Ti) implants with high osteogenic ability and consequent rigid osseointegration is a constant requirement from the clinic. In this study, we fabricate novel miRNA functionalized microporous Ti implants by lyophilizing miRNA lipoplexes onto a microporous titanium oxide surface formed by microarc oxidation (MAO). The microporous titanium oxide surface provides a larger surface area for miRNA loading and enables spatial retention of the miRNAs within the pores until cellular delivery. The loading of lipoplexes into the micropores on the MAO Ti surface is facilitated by the superhydrophilicity and Ti−OH groups gathering of the MAO surface after UV irradiation followed by lyophilization. A high miRNA transfection efficiency was observed in mesenchymal stem cells (MSCs) seeded onto the miRNA functionalized surface with no apparent cytotoxicity. When functionalizing the Ti surface with miR-29b that enhances osteogenic activity and antimiR-138 that inhibits miR-138 inhibition of endogenous osteogenesis, clear stimulation of MSC osteogenic differentiation was observed, in terms of up-regulating osteogenic expression and enhancing alkaline phosphatase production, collagen secretion and ECM mineralization. The novel miRNA functionalized Ti implants with enhanced osteogenic activity promisingly lead to more rapid and robust osseointegration of a clinical bone implant interface. Our study implies that lyophilization may constitute a versatile method for miRNA loading to other biomaterials with the aim of controlling cellular function.

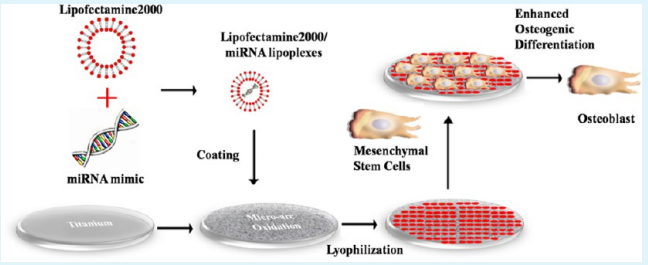

KEYWORDS: *microRNAs, lipoplexes, lyophilization, microarc oxidation, mesenchymal stem cells, titanium implants*

INTRODUCTION

Titanium (Ti) bone implants are widely used for replacement of bones, but further improvement is needed to meet clinical demands for faster and tighter osseointegration.[1] Micro- and nanoscale topographies can have favorable effects on implant osseointegration and some have already been applied in the clinic.[2−4] Nonetheless, the osteogenesis inducing ability from mere topography is supposed to be limited,[5] and thus additional cues should be implemented to render the implant more bioactive for better osseointegration. Instructive biomolecules like growth factors, morphogenetic agents, and DNA coding for them have been widely used to load onto various biomaterials, mainly for tissue engineering.[6−11] While different from the porous scaffolds, metal implant surfaces possess very limited reservoir capacity, so a pivotal issue is to increase the loading capacity of the Ti implant surface. Excitingly, the facile and economical microarc oxidation (MAO) treatment may provide a solution. The microstructure Ti surface formed by MAO has evenly distributed micropores and dramatically enlarged surface area for drug loading and retention. For example, the MAO Ti surface has already been used to load bone morphogenetic protein 2 (BMP-2) by physical adsorption and increased local bone formation has been observed,[12] demonstrating drug carrier potential of the MAO Ti surface. Furthermore, the MAO Ti surface itself possesses enhanced biological performance in terms of inducing apatite deposition and promoting osteoblast functions and has already been used in dental clinic.[13−15] Thus, superior bioactivity may be expected from the MAO Ti surface after loading with more advanced biomolecules with gene regulatory functions.

RNA interference is a valuable tool for targeted gene silencing by introducing small interfering RNAs (siRNAs) and/or microRNAs (miRNAs, miR) into the cytoplasm of cells. Compared to siRNAs that induce a more specific and usually more complete knockdown of target protein, miRNAs possess the ability to simultaneously silence a panel of genes albeit with relatively lower efficiencies.[16] In this way, miRNAs function the natural differentiation pathway and provide a potentially less harmful strategy to control differentiation of stem cells in vivo.[17,18] MicroRNAs participate in a wide range of cell functions including the control of proliferation, differentiation, apoptosis,

Received: January 28, 2013
Accepted: March 4, 2013
Published: March 4, 2013

Table 1. Primers Used for Real-Time PCR

gene	forward primer sequence (5′-3′)	reverse primer sequence (5′-3′)
COL1	GCCTCCCAGAACATCACCTA	GCAGGGACTTCTTGAGGTTG
ALP-2	AACGTGGCCAAGAACATCATCA	TGTCCATCTCCAGCCGTGTC
OCN	GGTGCAGACCTAGCAGACACCA	AGGTAGCGCCGGAGTCTATTCA
OSX	AAGGCAGTTGGCAATAGTGG	TGAATGGGCTTCTTCCTCAG
BMP	CAACACCGTGCTCAGCTTCC	TTCCCACTCATTTCTGAAAGTTCC
RUNX2	CCATAACGGTCTTCACAAATCCT	TCTGTCTGTGCCTTCTTGGTTC
GAPDH	GGCACAGTCAAGGCTGAGAATG	ATGGTGGTGAAGACGCCAGTA

Table 2. Contact Angles (deg) and Values of Surface Free Energy (mJ/m^2) of the MAO Ti Surface after Different Sterilization Methods

	contact angle (deg)			surface free energy (mJ/m^2)		
sterilization	distilled water	diiodomethane	formamide	total	polar	disperse
UV	11.77 ± 0.76	28.01 ± 0.57	0	68.77	40.71	28.06
ethanol	13.57 ± 1.47	39.70 ± 1.03	16.98 ± 0.13	67.72	44.19	25.53
autoclave	61.50 ± 1.27	44.08 ± 1.64	58.45 ± 2.47	40.98	14.63	26.35

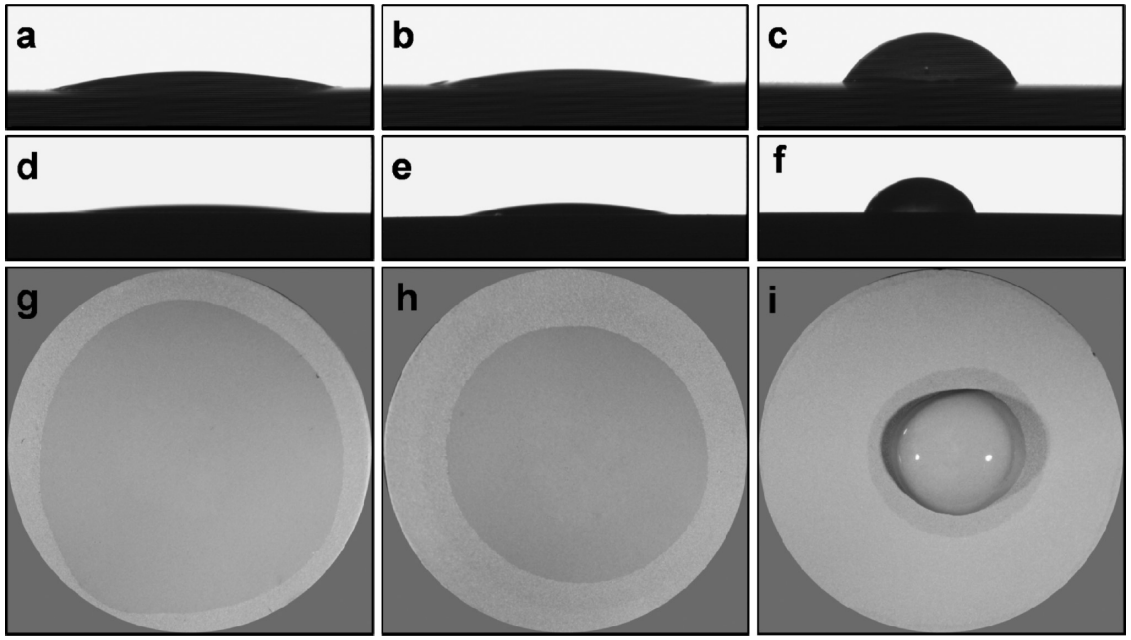

Figure 1. Water contact angles (a–c) and the lateral views (d–f) and the top views (g–i) of the miRNA lipoplex solution droplet on the MAO surface after different sterilization processes: (a, d, and g) UV irradiation, (b, e, and h) ethanol immersion, and (c, f, and i) autoclaving.

and other metabolic processes,[19] and they are capable of fostering the commitment of mesenchymal stem cells (MSCs) into tissues of various kinds.[16] Several reports have appeared describing the regulatory effect of miRNAs on osteogenesis.[20−24] Especially, miR-29b has been demonstrated to be a key regulator for the development of the osteoblast phenotype by targeting antiosteogenic factors such as histone deacetylase 4 and modulating bone extracellular matrix (ECM) proteins.[24] Besides up-regulating the osteogenesis promoting miRNAs, down-regulating endogenous levels of miRNAs that play a negative role in osteogenesis has also been demonstrated to promote osteogenesis.[25] For example, antimiR-138 has been shown to enhance in vivo bone formation by inhibiting miRNA-138.[22] Very recently, miRNAs have been shown to mediate the biological effects of biomaterial topographical cues on osteogenic differentiation of MSCs and osteoprogenitor cells.[26,27] Thus, miRNA levels are anticipated to be a robust target to promote biomaterial osseointegration. Even though there are already several efforts to load siRNAs to biomaterials to control cell commitment,[28,29] the application of miRNAs on Ti implants is still to be investigated.

In this study, we develop a novel miRNA functionalized microporous coating technique on Ti implant by lyophilizing miRNA lipoplexes onto the MAO Ti surface. On the basis of prior findings, we hypothesize that this system will possess multiple advantages including long-term stability,[29,30] enhanced substrate-mediated transfection possibly from the microporous MAO topography,[31−33] and the direct miRNA delivery to the adjacent bone tissues without arousing systemic side effects. The miR-29b and the antimiR-138 that are reported to promote osteogenic differentiation are chosen for functionalization of the Ti surface to obtain enhanced osteogenic activity. The surface morphology, miRNA localization, retention and integrity, stability on storage, transfection efficiency, and cytocompatibility were systemically studied and the efficacy to promote osteogenic differentiation of the miRNA functionalized microporous Ti

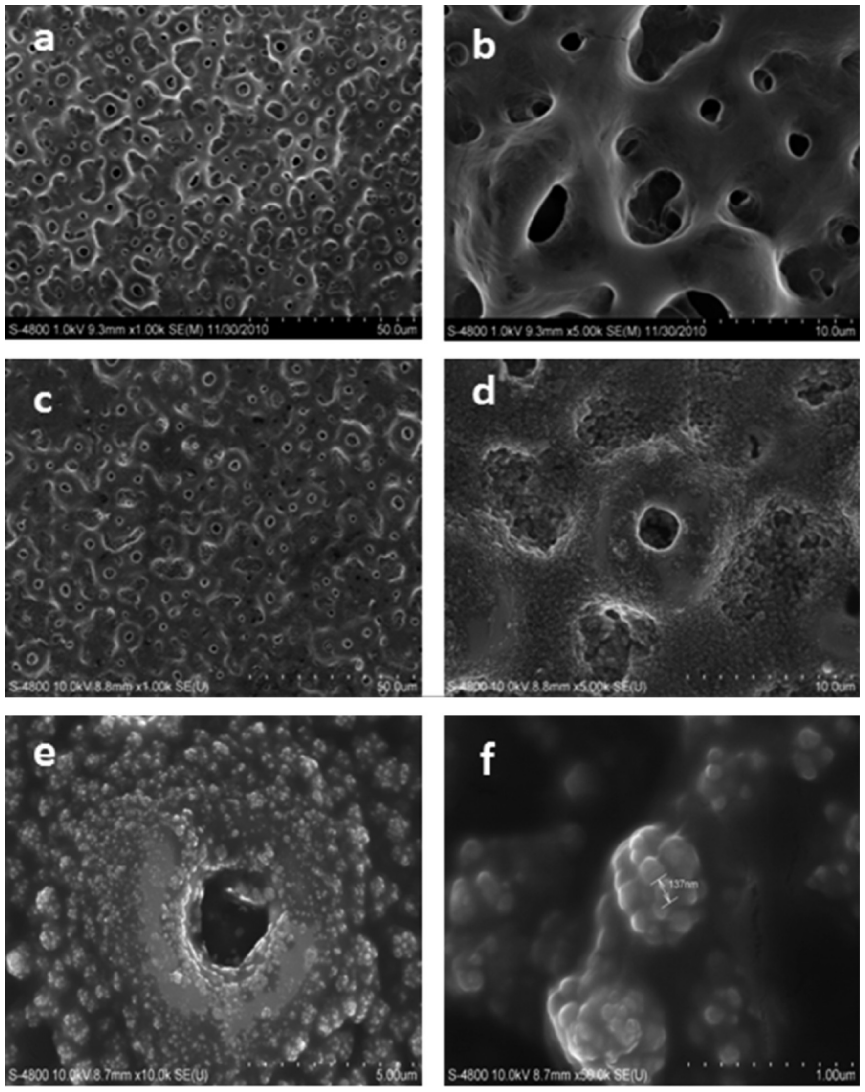

Figure 2. Morphology of the MAO Ti surfaces before and after miRNA lyophilization inspected by SEM: (a and b) pictures of different magnification for the naked MAO surface; (c–f) pictures with increasing magnification for the miRNAs functionalized MAO surface.

samples were systemically investigated. This study builds the foundation for advanced bone implants with enhanced osseointegration and provides meaningful experience for loading miRNAs to other biomaterials.

EXPERIMENTAL SECTION

Fabrication and Characterization of the miRNA Functionalized Microporous Surfaces. Commercially pure Ti discs (Φ 15 × 1.5 mm) were sequentially polished using waterproof abrasive paper of nos. 400–1200 and then ultrasonically cleaned in acetone, ethanol, and distilled water. The Ti discs were treated by a MAO process in an aqueous electrolyte containing 0.2 M calcium acetate monohydrate ($(CH_3COO)_2$—$Ca{\cdot}H_2O$) and 0.04 M sodium glycerophosphate ($C_3H_7Na_2O_6P{\cdot}5H_2O$) at 400 V DC for 5 min with a stainless steel plate as the cathode in a water-cooled bath.[34] After ultrasonic cleaning and drying, the samples were sterilized for 30 min. At this step, the influence of three different sterilization methods including autoclaving, ethanol immersion, and ultraviolet (UV) irradiation on sample surface hydrophilicity and miRNA loading was compared to optimize the sterilization procedure. Contact angle measurements and surface free energy calculation were conducted according to previous report.[34] The spreading of the miRNA lipoplex solution on the Ti surfaces was also observed.

The Lipofectamine2000/miRNA complexes were fabricated according to the manufacturer's instructions. Briefly, 1 μL Lipofectamine2000 and 2.5 μL 20 μM miRNAs were diluted with Opti-MEM to final volumes of 12.5 μL respectively and then mixed together. The 25 μL of Lipofectamine2000/miRNA complexes were plated on the MAO Ti surface and snap freezed for 5 min on dry ice followed by 24 h lyophilization at −40 °C resulting in Ti implants functionalized with 50 pmol miRNA. The surface morphology of the prepared samples was observed by field-emission scanning electron microscope (FE-SEM, Hitachi S-4800). Cy3-labeled miRNAs (Ribobio) were used to fabricate the coating in order to assess the miRNA loading. Immediately after fabrication or after 24 h of incubation in α modified minimum essential medium (α-MEM) supplemented with 10% fetal bovine serum (FBS), the samples were observed by a laser scanning confocal microscope layer by layer with an interlayer thickness of 200 nm (Fluo View, Olympus FV1000).

The integrity of the miRNA mimics miR-29b and the miRNA inhibitor antimiR-138 after packing by Lipofectamine2000 and lyophilization onto the Ti surface was tested using 20% urea–polyacrylamide gel electrophoresis. All the instruments and containers used were treated with Surface RNase Erasol (Tiandz). Briefly, the oligonucleotides on 10 miRNA functionalized Ti samples were extracted by 1 mL TRIzol reagent (Invitrogen). Afterward, 200 μL chloroform was added and the solution was centrifuged at 12 000 rpm for 15 min. After treatment with isopropanol and 75% alcohol, the miRNAs were

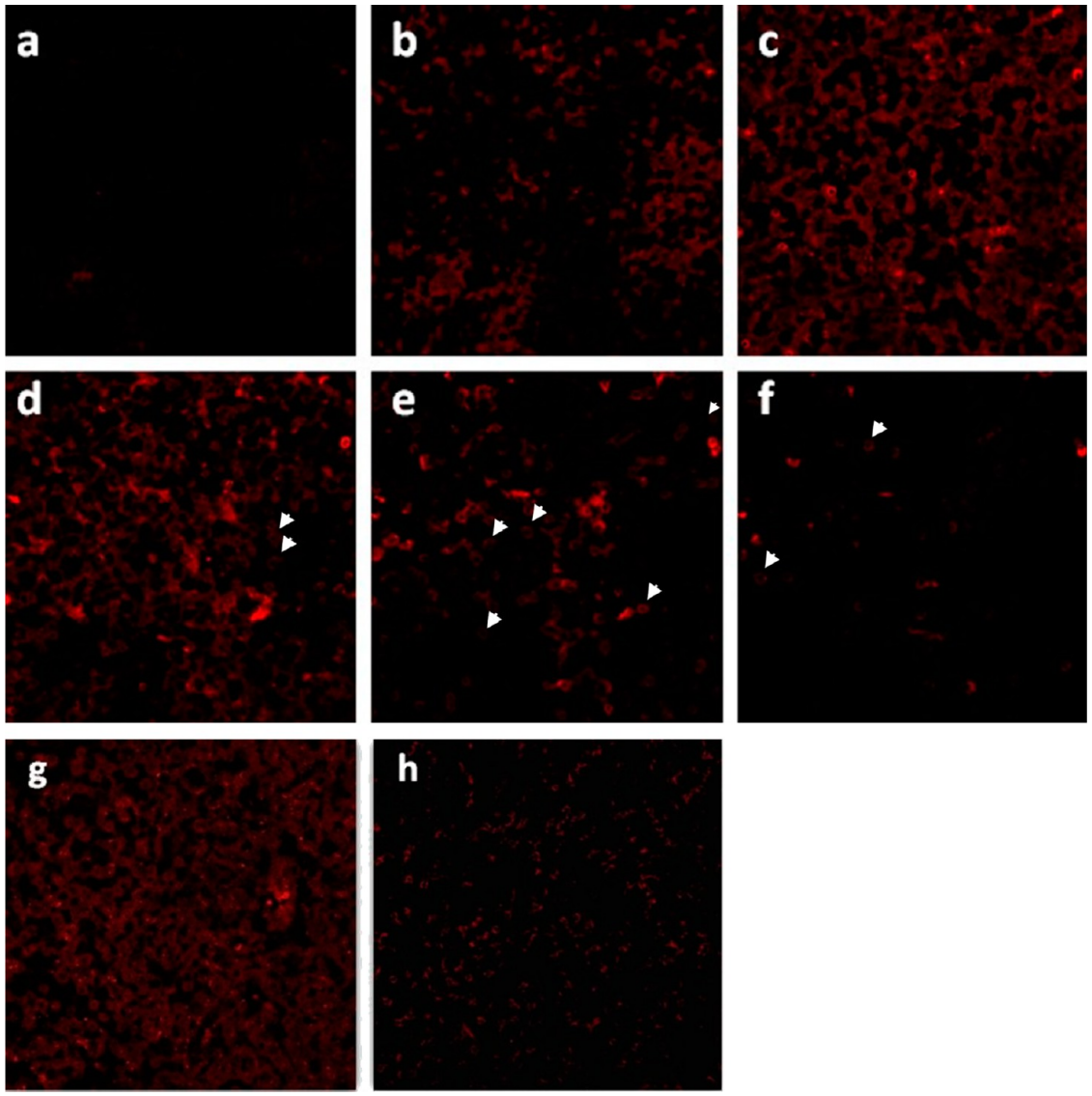

Figure 3. Fluorescence confocal laser scanning microscope of MAO surface functionalized with Cy3-labeled miRNAs: (a) the top layer starting to display fluorescence and (b–f) the continuing layers from top to down with a interlayer distance of 200 nm. The fluorescence images of Cy3-labeled miRNAs on the MAO surfaces at the same Z axis location before (g) and after (h) 24 h of incubation in cell culture medium at 37 °C.

isolated. Then 1 μg miRNA was loaded to perform the gel electrophoresis.

Cell Culture and Transfections. Primary rat bone marrow MSCs were obtained from 2-week-old Sprague–Dawley rats. The cells were cultured in α-MEM supplemented with 10% FBS and 1% penicillin/streptomycin and incubated in a humidified atmosphere of 5% CO_2 at 37 °C. The medium was replaced twice every week. Passages 2–4 were used in the experiment.

For the transfection of the lyophilized miRNAs on the Ti samples, 2.5×10^4 cells/cm^2 were inoculated on them placed in the 24 well plates and 24 h later, the medium was replaced with 500 μL fresh medium. For osteogenic induction, after 24 h incubation post-transfection, the cells were cultured with osteogenic medium containing 10 mM β-glycerophosphate (Sigma), 50 μg/mL ascorbic acid (Sigma) and 10^{-7} M dexamethasone (Sigma).

Transfection Efficiency Assay. To assess the transfection efficiency, Cy3-labeled miRNAs were used and the transfection was conducted as mentioned above. The transfected cells were harvested by trypsin, washed with phosphate buffered saline (PBS). The harvested cells were then centrifuged for 4 min at 3000 rpm, washed with PBS, centrifuged again, and finally fixed in 1% paraformaldehyde in PBS. The cells were processed on a flow cytometer (FACSVantage SE, BD Biosciences). Ten thousand cellular events were gated using forward and side scatter settings. The geometric mean of this population in the PerCP-Cy3 channel was used as a measure of Cy-3 fluorescence. Untreated MSCs served as the negative control. Each sample type was performed in three biological replicates.

Internalization of the miRNAs in cells was studied by fluorescence microscopy. Immediately after transfection, the cells were fixed with 4% paraformaldehyde and washed in PBS. The cell membrane was stained with 3,3′-dioctadecyloxacarbocyanine perchlorate (DIO). Then the DIO and Cy3 fluorescence signals were observed by the laser scanning confocal microscope.

Cell Viability. A cell count kit-8 (CCK-8, Beyotime) was employed in this experiment to quantitatively evaluate cell viability.[35] Briefly, after 24 h of culture in the regular medium post-transfection, the culture medium was removed, and the cultures were washed with PBS twice. Then 360 μL serum-free α-MEM medium and 40 μL CCK-8 were added to each well, followed by incubation at 37 °C for 3 h. The supernatant was transferred to a 96-well plate, and the optical density (OD) at 450 nm was determined using a spectrophotometer (Biotek). The MAO surface and tissue culture plate served as control and the cells were cultured on them using the same procedures as on the miRNA

functionalized microporous Ti samples. Three parallel experiments in each group were used to assess the cell viability.

Lactate Dehydrogenase Activity Assay. The lactate dehydrogenase (LDH) activity was used as an index of cytotoxicity in the culture medium. Succinctly, after 24 h of culture post-transfection, the culture medium was collected and centrifuged and the supernatant was used for the LDH activity assay. The LDH activity was determined spectrophotometrically according to the manufacturer's instructions. Three parallel experiments in each group were conducted.

Cell Morphology. MSCs were seeded at a density of 5×10^4 cells/well. After 24 h of incubation post-transfection, the samples with cells cultured on them were washed with PBS, fixed in 2.5% glutaraldehyde, dehydrated in a graded ethanol series and freeze-dried. After sputter coating with gold, the cell morphology was observed by the FE-SEM.

Osteogenesis-Related Gene Expression. The expression of osteogenesis-related genes was evaluated using the real-time polymerase chain reaction (real-time PCR). The cells were seeded with 5×10^4 cells/well. After 24 h of incubation in the fresh medium post-transfection, the medium was changed into osteogenic medium and cultured for 7 and 14 days. Total RNA was isolated using the TRIzol reagent (Invitrogen). Then 2 μg RNA from each sample was reversed transcribed into complementary DNA (cDNA) using the PrimeScript RT reagent kit (TaKaRa). Expression of osteogenesis-related genes including collagen type I α 1 (COL1), runt-related transcription factor 2 (RUNX2), alkaline phosphatase (ALP), BMP-2, osterix (OSX), and osteocalcin (OCN) was quantified using real-time PCR. PCR reaction was carried out using SYBR Premix Ex Taq II (TaKaRa) on the CFX96 real-time PCR System (Biorad). The relative expression levels for each gene of interest were normalized to that of the housekeeping gene GAPDH. The PCR primers were synthesized as shown in Table 1.

ALP Staining. The cells were inoculated at a density of 5×10^4 cells/well and cultured as in the real-time PCR assay. After culturing for 7 and 14 days, the cells were washed with PBS and fixed, and ALP was stained with the BCIP/NBT ALP color development kit (Beyotime) for 15 min. The samples were washed thoroughly with PBS to acquire the images.

Collagen Secretion. The cells were inoculated at a density of 5×10^4 cells/well and cultured the same as in the ALP staining assay. After culture of 7 and 14 days in the osteogenic medium, the cultures were washed by PBS and fixed by 4% paraformaldehyde. Then, the collagen secretion was stained by 0.1 wt % Sirius red (Sigma) in saturated picric acid for 18 h. The unbound stain was removed in 0.1 M acetic acid, and then, the images were collected. To quantitatively assess the collagen secretion, the stain on the samples was eluted in 500 μL destain solution (0.2 M NaOH/methanol 1:1) and the optical density at 540 nm was measured using a spectrophotometer.

ECM Mineralized Nodule Displaying. The cells were cultured in a similar way as in the collagen secretion assay. After culturing for 14 and 28 days, the cells were washed twice with PBS and then fixed with 60% isopropanol for 1 min. After rehydrating with distilled water for 2–3 min, the ECM mineralized nodules formed by MSC culture were stained with 1 wt % alizarin red (Sigma) for 3 min. After thorough washing with distilled water, the images were taken. For the quantitative analysis, the stain was dissolved in 10% cetylpyridinum chloridein 10 mM sodium phosphate (pH = 7), and the absorbance was measured at 620 nm.

Statistical Analysis. The one way ANOVA and Turkey post hoc tests were used to determine the level of significance. $p < 0.05$, 0.01, and 0.001 was set to be significant, highly significant, and extremely significant, respectively.

RESULTS

Optimization of the Sterilization Method for miRNA Loading. Different sterilization methods are reported to alter the surface properties of the Ti samples, especially hydrophilicity;[36] thereby influencing the miRNA loading process. We compared the influence of three commonly used sterilization methods on the hydrophilicity of MAO Ti surface and miRNA loading. As shown in Table 2 and Figure 1, parts a, b, and c, autoclaving gave rise to largest water contact angle of 61.5° and lowest surface energy of 40.98 mJ/m^2 compared to UV irradiation and ethanol immersion, which led to much smaller water contact angles of 11.77° and 13.57° and higher surface energy of 68.77 and 67.72 mJ/m^2, respectively. Drops of miRNA lipoplex solution yielded the same contact angles as water on the Ti surface sterilized with different methods (data not shown). UV irradiation induced the smallest contact angle followed by ethanol immersion and autoclaving led to much bigger contact angle. From the top view, we observed that on the UV sterilized surface the miRNA lipoplex droplet spread well nearly fully covering the Ti surface (Figure 1g), while on the ethanol sterilized surface the spreading of the droplet was worse (Figure 1h) and the autoclaved surface resulted in the worst spreading (Figure 1i). Hence, UV sterilization was chosen for the following experiment.

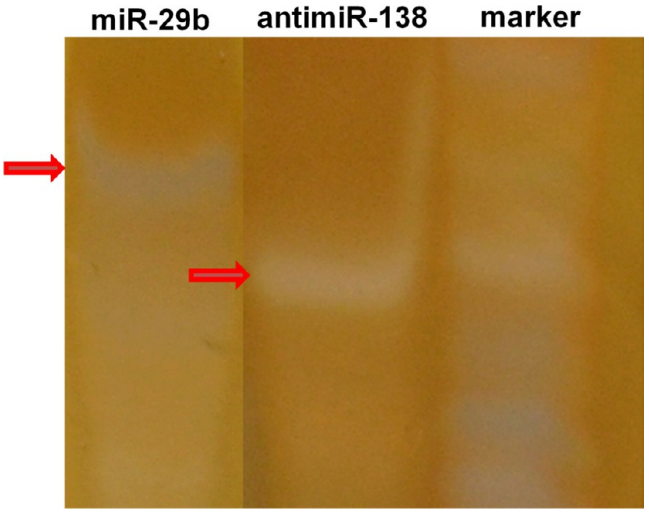

Figure 4. Electrophoresis of the miR-29b and antimiR-138 after retrieved from the miRNA functionalized microporous coatings. The red arrows indicate the location of the RNA bands.

Characterization of the miRNA Functionalized Microporous Surfaces. The morphology of the MAO Ti surfaces before and after miRNA lyophilization was characterized by the FE-SEM (Figure 2). The MAO surface has a microporous structure with the pore diameter varying between 2 and 5 μm, which greatly increases the surface area of the Ti sample (Figure 2, parts a and b). For the miRNA functionalized MAO Ti surface, the miRNA lipoplexes distribute evenly along the microporous titanium oxide surface (Figure 2c). They fill out some of the smaller pores and slightly decrease the diameters of the bigger pores by attaching to their walls. The higher magnification pictures clearly demonstrate that the lipoplexes enter into the pores and attach to the walls (Figure 2, parts d and e). Higher magnification pictures reveal the sizes of the lipoplexes to be around 140 nm (Figure 2f).

To observe the miRNA retention and localization on the MAO Ti surface, the Cy3-labeled miRNAs were applied in the functionalization process of the Ti surface and followed by inspection by the laser scanning confocal microscopy. The miRNA functionalized surface was scanned layer by layer from the surface to bottom of the cavities with 200 nm intervals (Figure 3, parts a–d). The fluorescence images further corroborate that the miRNA lipoplexes enter into the pores and distribute on the surface. A minor fraction of the miRNA is deposited on the top surface layer of functionalized microporous surface (Figure 3a) whereas more miRNA is deposited in the deeper sections of the microporous titanium oxide surface (Figure 3, parts b–e). From Figure 3d, we can observe many

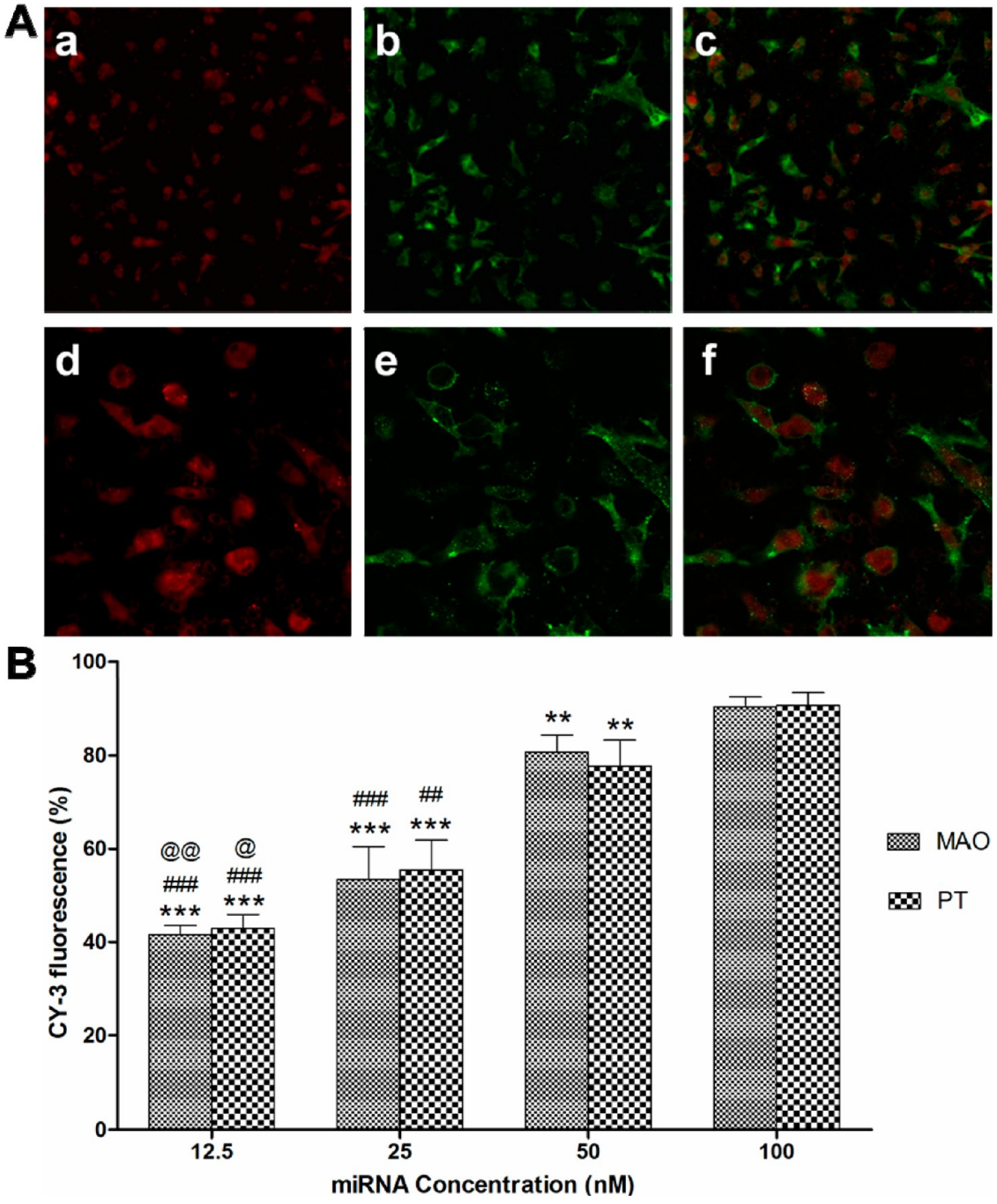

Figure 5. (A) Fluorescence images of 20× (a–c) and 40× (d–f) showing the uptake of miRNAs by cells after 24 h of culture on the miRNA functionalized MAO surface: (a and d) Cy3-labeled miRNAs (red color), (b and e) cell membrane stained by DIO (green color), and (c and f) the merged images. (B) Comparison of the transfection efficiency between the miRNA functionalized MAO and flat polished Ti (PT) surfaces by flow cytometry. (** and ***) $p < 0.01$ and 0.001 vs the 100 nM miRNA functionalized surface; (##, ###) $p < 0.01$ and 0.001 vs the 50 nM miRNA functionalized surface; (@, @@) $p < 0.05$ and 0.01 vs the 25 nM miRNA functionalized surface.

fluorescenced rings as indicated by the white arrows further increasing in Figure 3e, which is the indication for the distribution of the miRNAs on the walls of the pores. Figure 3f shows that the near bottom layer also exhibits miRNA functionalized coating. It can be estimated that the total thickness of the miRNA layer on the functionalized microporous surface is about 1000 nm. To measure the release rate, the same Z-stack was measured before (Figure 3g) and after 24 h immersion in the culture medium (Figure 3h). A substantial amount of miRNA is retained in the pores even after 24 h of immersion in the culture medium, indicating good retention of the lipocomplexes.

To analyze the stability of the oligonucleotides on the surface miR-29b and antimiR-138 were retrieved from the functionalized microporous surfaces and subjected to gel electrophoresis (Figure 4). The observation of distinct RNA bands corresponding to intact oligonucleotides suggests that the oligonucleotides remain stable after lyophilizing onto the Ti surface.

Transfection Efficiency of the miRNA Functionalized Microporous Surfaces. To visualize the internalization of the

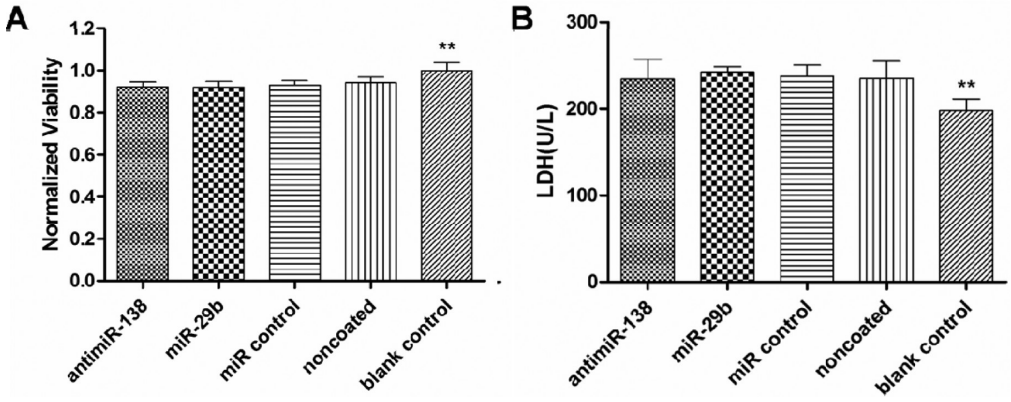

Figure 6. (A) Cell viability measured by CCK-8 at 24 h after transfection and (B) LDH amount released by cells during the first 24 h after transfection. (**) $p < 0.05$ compared with the other four groups.

miRNAs to cells, the Cy3-labeled antimiR-138 was applied in the coating process before seeding and growing MSCs on the surface for 24 h. Fluorescent microscopy clearly shows that miRNAs mainly locate in the cell body of all cells, suggesting successful uptake of the miRNAs by the cells and a high transfection efficiency (Figure 5A; miRNA appears as a red color, and the cell membrane is stained green). We also notice some fluorescenced rings, which presumably are the undelivered miRNAs in the pores on the MAO surface.

The transfection efficiency was more accurately assessed by flow cytometry (Figure 5B). The transfection efficiency increases with the miRNA concentrations on the coatings. At 100 nM, a transfection efficiency as high as 90% is achieved.

Cell Viability and Cytotoxicity. The viability of cells cultured for 24 h post-transfection was assessed using Cell Counting Kit-8 (CCK-8) (Figure 6A). Compared to the naked MAO surface, functionalization with miR-29b, antimiR-138, or miR control did not influence the cell viability. The amount of LDH released by cells grown on the various surfaces was also used as an indicator to evaluate cytotoxicity (Figure 6B). None of the Ti samples functionalized with miR-29b, antimiR-138, and miR control exhibit any apparent cytotoxicity compared to the naked MAO sample.

Cell Morphology. The cell morphology was investigated by FE-SEM (Figure 7). Generally, the cells show very similar cell morphology when grown on the naked MAO surface indiscriminately of any oligonucleotide functionalization. The cells spread out with abundant lamellipodia and filopodia, bridging over the concave areas on the porous Ti surface and anchoring themselves to the substrate via the cell podia.

Osteogenic Gene Expression. The expression levels of osteogenic genes were assessed by real-time PCR (Figure 8). Generally, the antimiR-138 and the miR-29b functionalized surfaces generate higher expression of multiple genes than the miR control surface, the naked MAO surface as well as the blank control. For the genes BMP, OCN, OSX, and RUNX2, the antimiR-138 functionalized surface induces higher expression than the miR-29b functionalized surface. For COL1, at day 7, the miR-29b functionalized surface induces higher expression than using antimiR-138, whereas this trend is reversed after 14 days of culture. For ALP, the miR-29b functionalized surface induces higher expression than the antimiR-138 functionalized surface for both time points.

ALP Production. The MSCs produced high amounts of ALP on all the substrates after 7 days of osteogenic induction whereafter it seems to decline over time (Figure 9). At day 7, both the naked MAO surface and the miR control functionalized surface induced similar levels of ALP production and the antimiR-138 and the miR-29b functionalized surfaces generated much higher one. Notably, at day 14 both the antimiR-138 and the miR-29b functionalized surface and miR control displayed a punctuated ALP pattern. A significantly larger area was covered when the surface was functionalized antimiR-138 and in the presence of miR-29b the entire surface was almost covered with ALP.

Collagen Secretion. Next the collagen secretion was assessed by Sirius red staining (Figure 10). The optical images show that the MSCs secrete collagen in a dotted pattern after 7 days of culture on the naked MAO surface. Less collagen was secreted on the miR control functionalized MAO surface, while the antimiR-138 and the miR-29b functionalized surfaces induced much denser collagen secretion to a level comparable to or slightly higher than the naked MAO surface. After 14 days of culture, there was still sporadic collagen dots on the naked MAO surface and the miR control functionalized MAO surface, whereas the antimiR-138 and the miR-29b functionalized surfaces exhibited much more intensive collagen dots. Quantification of the results revealed that the miR control functionalized MAO surface induced about half of the amount of collagen compared the naked MAO surface at day 7 and a similar amount at day 14. The antimiR-138 and the miR-29b functionalized surfaces yielded similar or slightly higher collagen production than the naked MAO surface at day 7, but, importantly, at day 14 they induced 2 times more than the naked MAO surface.

ECM Mineralization. Production of ECM mineralized nodules was assessed with alizarin red, and the results are shown in Figure 11. Mineralized nodule formation can be observed by the MSCs after 14 days of culture on the naked MAO surface. Slightly smaller and more lightly stained mineralized nodules were generated by the miR control functionalized MAO surface. The antimiR-138 and the miR-29b functionalized surfaces induced dramatically denser and larger mineralized nodules than the naked MAO surface. A similar trend was observed up to 28 days of incubation.

DISCUSSION

Implants exhibiting more robust osseointegration will be essential for clinical use. Loading the biomaterial with therapeutic oligonucleotide that can promote this process at the genetic level is a promising approach. There are numerous efforts to load

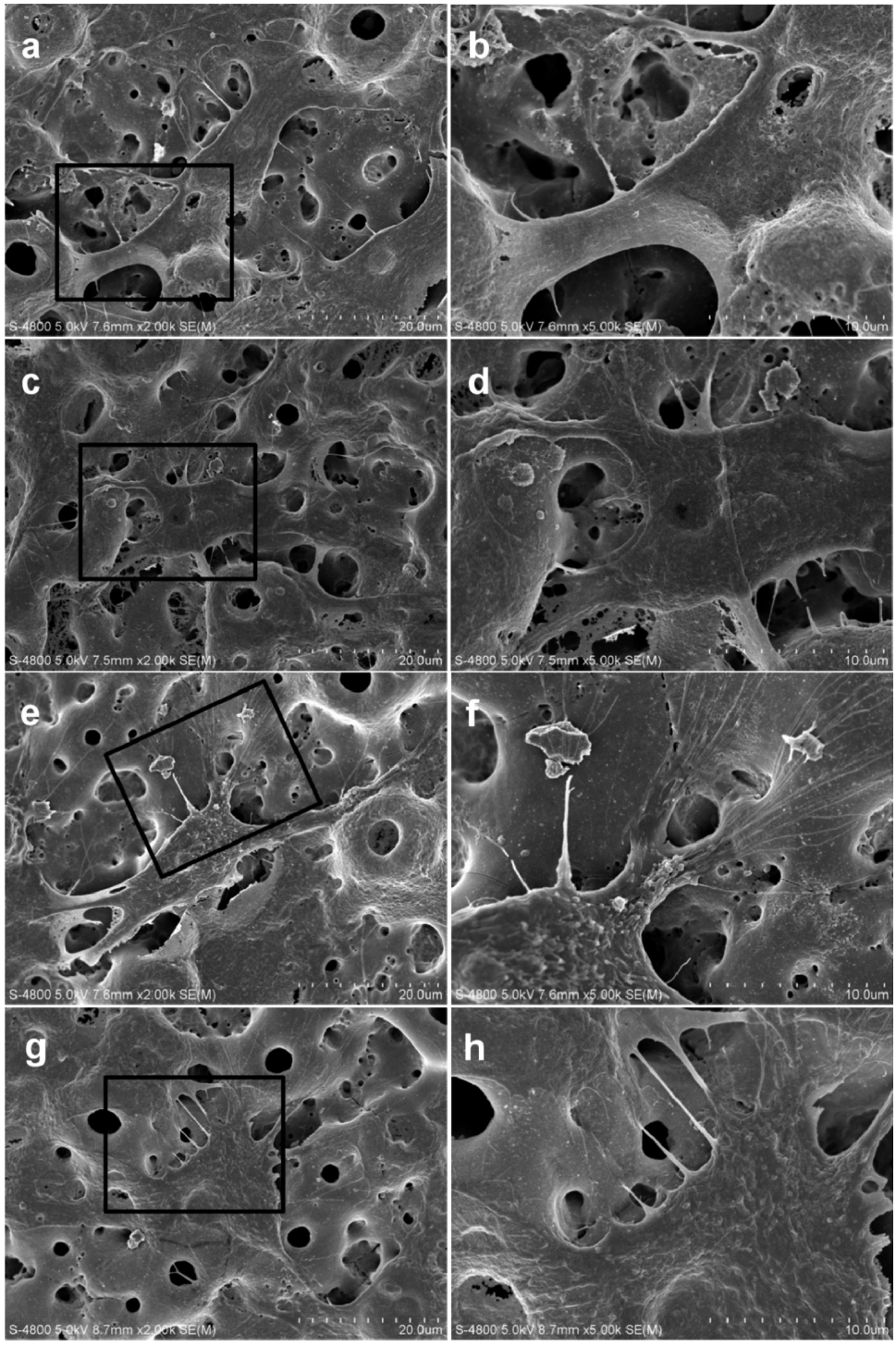

Figure 7. SEM pictures showing the cell morphology after 24 h of incubation after transfection on different samples: (a and b) the antimiR-138 functionalized MAO surface, (c and d) the miR-29b functionalized MAO surface, (e and f) the miR control functionalized MAO surface, and (g and h) the naked MAO surface.

DNA and siRNAs onto biomaterials to promote specific commitment of cells,[28,29,33] while there is still no such attempt for miRNAs. We herein demonstrate the miRNA functionalized microporous coatings on Ti implant as a feasible route to create a reservoir for miRNAs and to deliver to surrounding cells.

Lyophilization constitutes a feasible strategy to load the miRNA lipoplexes onto the MAO Ti surface. However, the miRNA lipoplex loading need to be conducted after sample sterilization so it is important to study how this process influences the physical characteristics of the Ti surface such as wettability and in turn the lipoplex loading process.[36] In contrast to the other sterilization methods, UV irradiation tailors the MAO Ti surface to be superhydrophilic due to the formation of abundant basic Ti−OH groups,[37] which facilitates the spread of the miRNA lipoplex-containing solution on the Ti surface. Using the laser scanning confocal microscopy, we disclosed that the miRNA lipoplexs indeed entered more deeply into the holes and appeared denser on the inner walls. The FE-SEM pictures

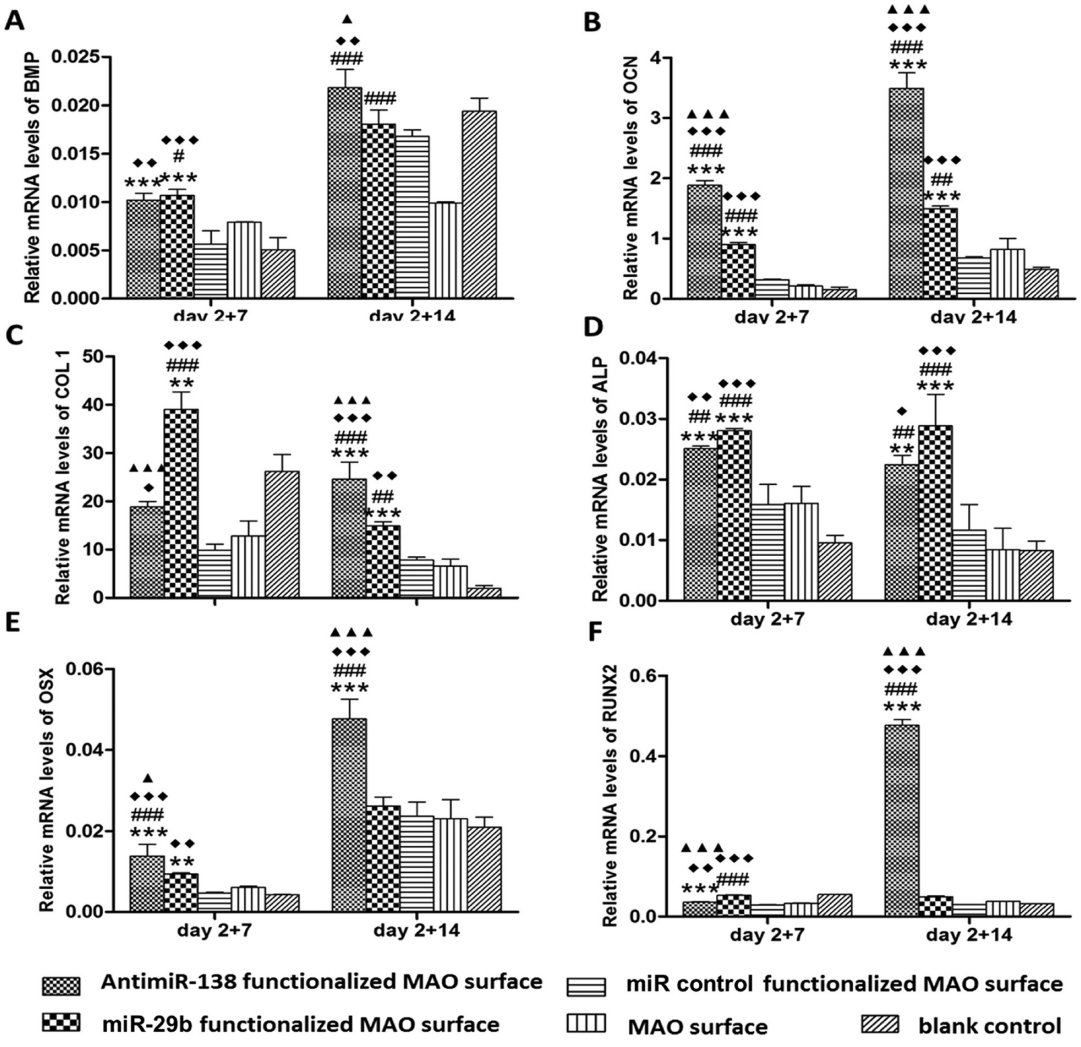

Figure 8. Relative expressions of (A) BMP, (B) OCN, (C) Col1, (D) ALP, (E) OSX, and (F) RUNX2 by MSCs cultured on different samples. After transfection, the medium is changed into fresh medium and the cells are cultured for another 24 h. Then the medium is changed into osteogenic medium and cultured for 7 and 14 days. All values are normalized to GAPDH. (**, ***) $p < 0.01$ and 0.001 vs the blank control; (#, ##, ###) $p < 0.05$, 0.01, and 0.001 vs the naked MAO surface; (♦,♦♦, ♦♦♦) $p < 0.05$, 0.01, and 0.001 vs the miR control functionalized MAO surface; (▲, ▲▲, ▲▲▲) $p < 0.05$, 0.01, and 0.001 vs the miR-29b functionalized MAO surface.

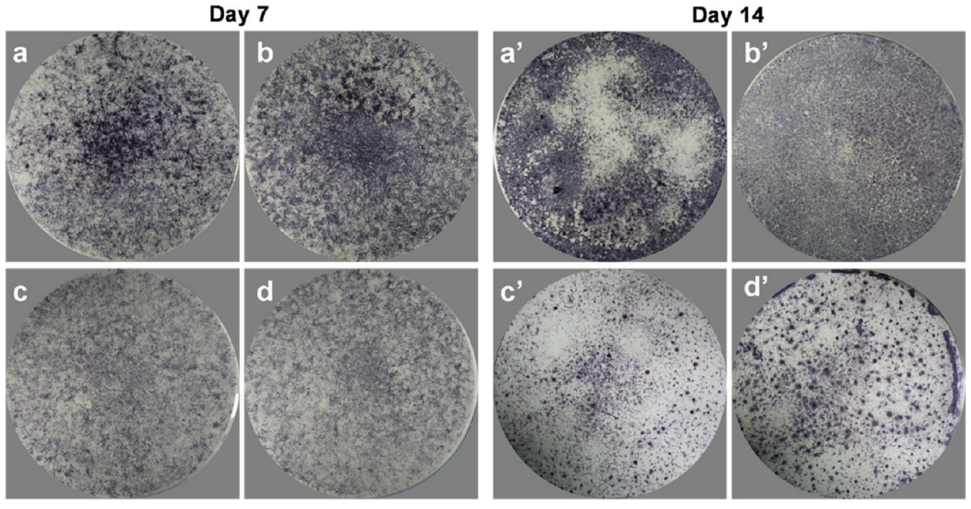

Figure 9. ALP staining of MSCs after 7 and 14 days of culture in the osteogenic medium: (a and a′) the antimiR-138 functionalized MAO surface, (b and b′) the miR-29b functionalized MAO surface, (c and c′) the miR control functionalized MAO surface, and (d and d′) the naked MAO surface.

dx.doi.org/10.1021/am400374c | ACS Appl. Mater. Interfaces 2013, 5, 2733−2744

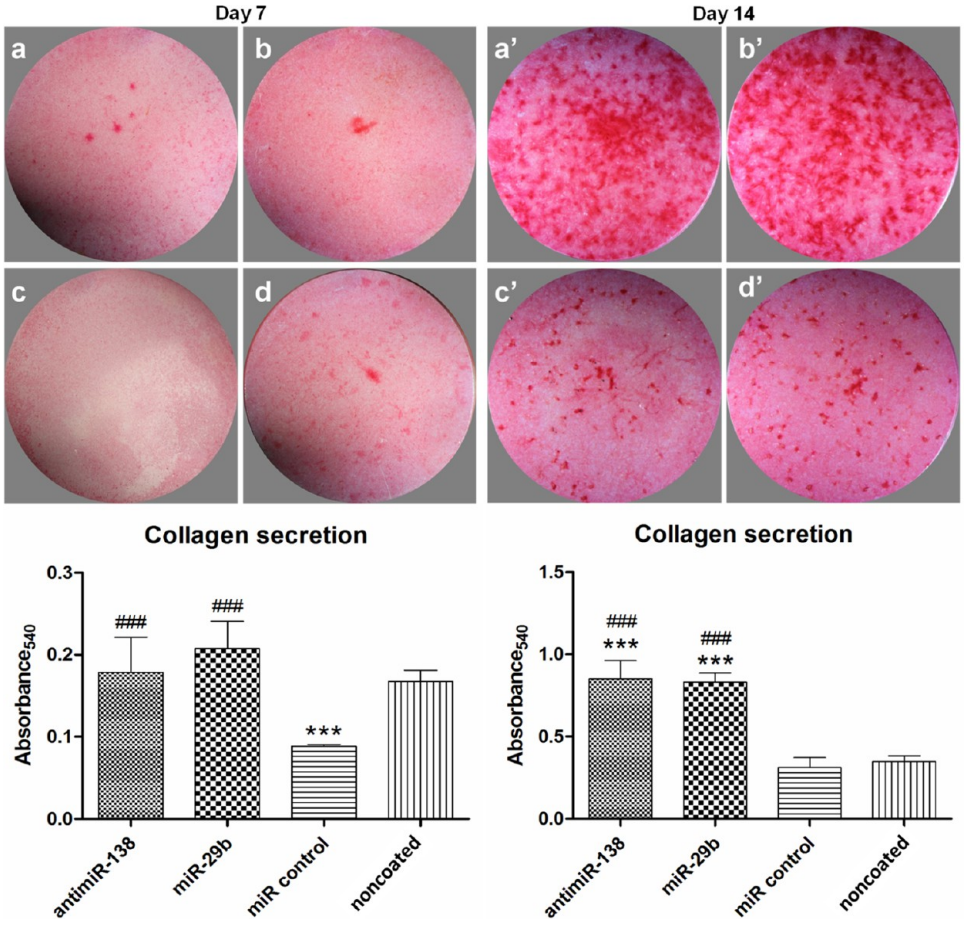

Figure 10. Staining of collagen secreted by MSCs after 7 and 14 days of culture in the osteogenic medium: (a and a′) the antimiR-138 functionalized MAO surface, (b and b′) the miR-29b functionalized MAO surface, (c and c′) the miR control functionalized MAO surface, and (d and d′) the naked MAO surface. The upper panel lists the optical images, and the lower panel shows the quantitative colorimetric results. (***) $p < 0.001$ vs the naked MAO surface; (###) $p < 0.001$ vs the miR control functionalized MAO surface.

revealed that the lipoplexes distributed relatively evenly with intact structures and an average diameter of 140 nm. It should be bear in mind that no lyoprotectant was used in the current study to avoid unwanted side effects from them. This is important since ordinary lyoprotectants, such as glucose, can interfere with the cell differentiation.[38] The result is in agreement with previous report that lipoplexes can function well after being freeze-dried without the need for lyoprotectant.[29] We observed the strong attachment of the lipoplexes to the Ti substrate. We also assessed the integrity of the miRNAs lyophilized to the Ti surface and found that the miRNAs remain intact for extended time intervals on the Ti surface. This is important for sufficient shelf life in an industrial production and clinical application. Previously we found that the lyophilized miRNAs on a surface possess good stability on storage. When stored at 4 or −20 °C, no obvious decrease in the miRNA transfection efficiency after even 3 month storage was observed (unpublished data).

The miRNA functionalized microporous surface is able to result in high cell uptake and transfection efficiency. There are still some miRNAs retained in the pores after 24 h of incubation with cells, which may provide a pool for a more sustained transfection. The transfection efficiency of the coatings is positively dependent on the miRNA content and a high transfection efficiency of up to 90% is reached for the sample with 100 nM miRNAs, which is correlated with cell uptake demontrated by the fluorescence images in Figure 5A, that nearly all the cells have miRNAs in their body. The high transfection efficiency can be attributed to the substrate-mediated transfection,[33] which refers to immobilizing transfection agents on a solid surface and then delivering them locally to the attached cells.[39] Compared to the conventional transfection, the substrate-mediated transfection enables direct contact between the transfection agents and cells and reducing the amount of floating miRNA which is not in contact with cells thereby improving the transfection efficiency.[33] Recently, there is emerging evidence indicating the effect of surface micro- and nanotechnology on endocytosis and thus nonviral gene delivery.[31,32,40] To determine the potential contribution of the MAO microporous surface to the transfection efficiency, we compared the transfection efficiency of the miRNA functionalized microporous surface with that of the flat counterpart (Figure 5B). We observed no apparent difference in the transfection efficiency of the two coatings, excluding the possible contribution of the microporous surface to the transfection efficiency.

An elementary requirement for a bone implant is good cytocompatibility, and our data demonstrate that the miRNA functionalized microporous surfaces satisfy this requirement. The cationic lipids are reported to induce toxicity by inhibiting important proteins like PKC in cells.[41] Compared to the naked MAO surface, the miRNA functionalized microporous surfaces

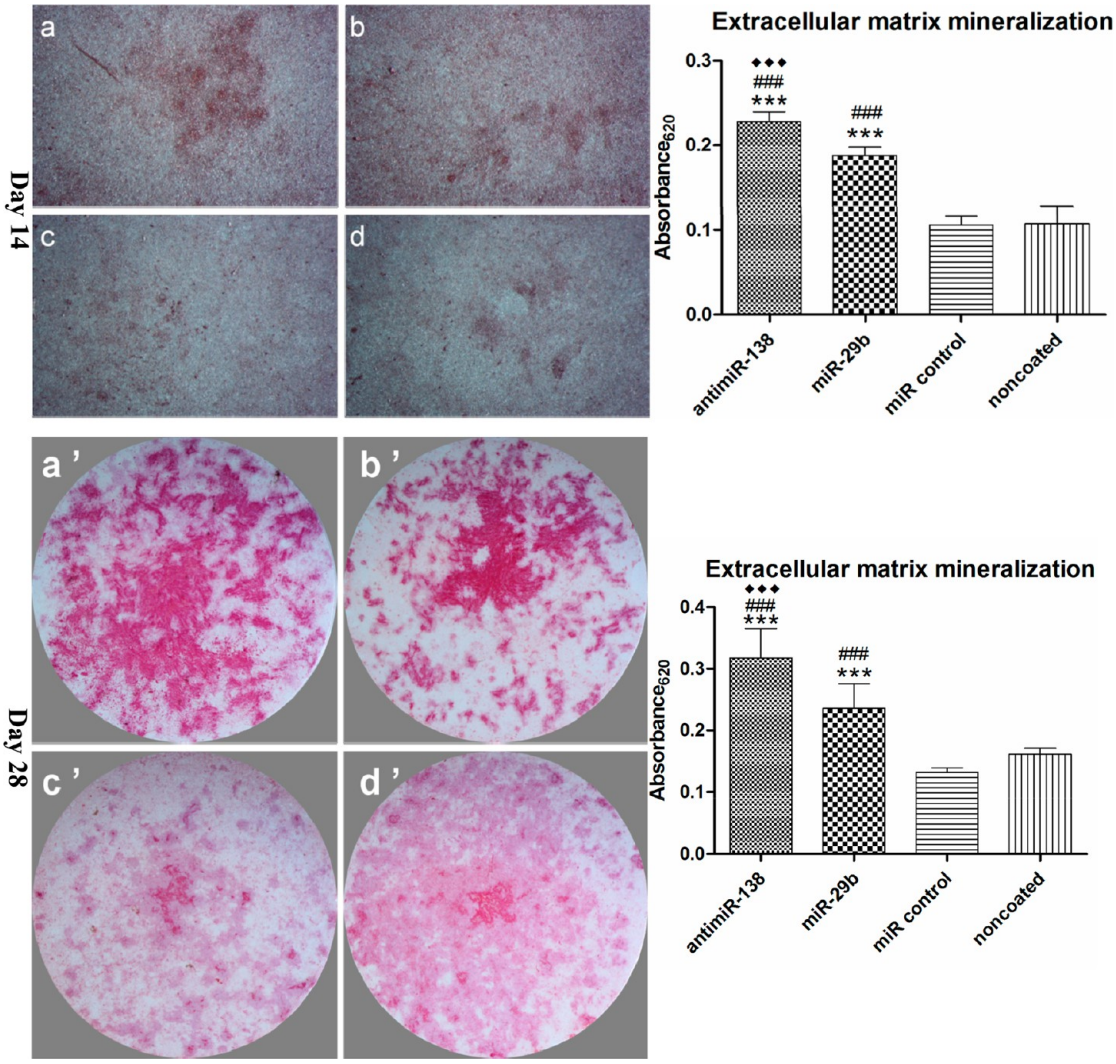

Figure 11. Staining of ECM mineralized nodules formed by MSCs after 14 days of culture in the osteogenic medium: (a) the antimiR-138 functionalized MAO surface, (b) the miR-29b functionalized MAO surface, (c) the miR control functionalized MAO surface, and (d) the naked MAO surface. The right panel shows the semiquantitative results. (***) $p < 0.001$ vs the naked MAO surface; (###) $p < 0.001$ vs the miR control functionalized MAO surface; (◆◆◆) $p < 0.001$ vs the miR-29b functionalized MAO surface.

induce comparable levels in the cell viability and LDH release, indicating good cytocompatibility. On the contrary, the siRNA lyophilized reverse transfection formulations have been observed to induce 30−45% reduction in cell viability.[42] This evidence may support the idea that miRNAs are more biologically friendly than siRNAs. Besides, the absence of cytotoxicity from the miRNA functionalized microporous surfaces may be also ascribed to a delayed delivery of the miRNA lipoplexes. Good attachment and spread of cells on the implant surface is pivotal for the ensuing cell functions. On all the Ti samples, the cells spread well with abundant lamellopodia and filopodia stretching out to anchor to the microporous titanium oxide surface, which again illustrates that the miRNA lipoplexes possess good cytocompatibility without impeding the biological effects from the sample topography.

Here we observed that the antimiR-138 and the miR-29b functionalized microporous surfaces led to enhanced osteogenic activity represented by the up-regulation of osteogenic gene expression, enhanced ALP and collagen production, and ECM mineralization. Overexpression of miR-138 inhibits in vitro osteoblast differentiation of MSCs and in vivo ectopic bone formation, and inhibition of miR-138 function by antimiR-138 promotes expression of osteogenic genes, ALP activity, and ECM mineralization of MSCs and in vivo ectopic bone formation.[22] miR-29b can promote osteogenesis by targeting antiosteogenic factors such as histone deacetylase 4 and by modulating bone ECM proteins.[24] Our results are in accordance with these reports. Though the lipoplex loading does not impair the cell adhesion and spread as above-mentioned, the data from the miR control functionalized surface indicate that Lipofectamine2000 indeed impairs MSC ostogenic differentiation. Better bioactivity may be expected when more suitable nonviral vectors are tested in the future.

■ CONCLUSIONS

We show a novel miRNA functionalized microporous Ti implant by lyophilizing the miRNA lipoplexes onto the microporous titanium oxide surface formed by MAO. The lipoplexes can be evenly loaded onto the MAO Ti surface and into the micropores. The oligonucleotides maintain their structural integrity without apparent degradation after lyophilization onto the Ti surface. High miRNA transfection in MSCs is achieved without apparent

cytotoxicity. The Ti implants functionalized with miR-29b and antimiR-138 obviously enhance osteogenic differentiation of MSCs, thus being very promising to expedite clinical implant osseointegration. The study also provides meaningful experience for miRNA loading to other biomaterials.

AUTHOR INFORMATION

Corresponding Author

*E-mail: zhaolingzhou1983@hotmail.com (L.Z.); wqtzym@fmmu.edu.cn (Y.Z).

Present Address

⊥S.G.: Kunshan RNAi Institute, Kunshan, Jiangsu 215300, China.

Author Contributions

‖K.W. and W.S. are cofirst authors.

Notes

The authors declare no competing financial interest.

ACKNOWLEDGMENTS

This study was granted by National Natural Science Foundation of China Nos. 31200716, 81070862, and 31170915. The grants from The Fourth Military Medical University and School of Stomatology, The Fourth Military Medical University, to L.Z. are also appreciated.

REFERENCES

(1) Beutner, R.; Michael, J.; Schwenzer, B.; Scharnweber, D. *J. R. Soc. Interface* **2010**, *7*, S93−S105.

(2) Buser, D.; Broggini, N.; Wieland, M.; Schenk, R. K.; Denzer, A. J.; Cochran, D. L.; Hoffmann, B.; Lussi, A.; Steinemann, S. G. *J. Dent. Res.* **2004**, *83*, 529−33.

(3) Park, J. W.; Jang, J. H.; Lee, C. S.; Hanawa, T. *Acta Biomater* **2009**, *5*, 2311−21.

(4) Telleman, G.; Albrektsson, T.; Hoffman, M.; Johansson, C. B.; Vissink, A.; Meijer, H. J.; Raghoebar, G. M. *Clin. Implant Dent. Relat. Res.* **2010**, *12*, 153−60.

(5) Kilian, K. A.; Bugarija, B.; Lahn, B. T.; Mrksich, M. *Proc. Natl. Acad. Sci. USA* **2010**, *107*, 4872−4877.

(6) Liu, Y.; de Groot, K.; Hunziker, E. B. *Bone* **2005**, *36*, 745−57.

(7) Wildemann, B.; Lubberstedt, M.; Haas, N. P.; Raschke, M.; Schmidmaier, G. *Biomaterials* **2004**, *25*, 3639−44.

(8) Huang, Y. C.; Simmons, C.; Kaigler, D.; Rice, K. G.; Mooney, D. J. *Gene Ther.* **2005**, *12*, 418−26.

(9) Jang, J. H.; Rives, C. B.; Shea, L. D. *Mol. Ther.* **2005**, *12*, 475−83.

(10) Lee, S. J. *Yonsei Med. J.* **2000**, *41*, 704−19.

(11) De Laporte, L.; Shea, L. D. *Adv. Drug Deliv. Rev.* **2007**, *59*, 292−307.

(12) Wikesjo, U. M.; Qahash, M.; Polimeni, G.; Susin, C.; Shanaman, R. H.; Rohrer, M. D.; Wozney, J. M.; Hall, J. *J. Clin. Periodontol.* **2008**, *35*, 1001−10.

(13) Han, Y.; Xu, K. *J. Biomed. Mater. Res. A* **2004**, *71*, 608−14.

(14) Zhang, Y. M.; Bataillon-Linez, P.; Huang, P.; Zhao, Y. M.; Han, Y.; Traisnel, M.; Xu, K. W.; Hildebrand, H. F. *J. Biomed. Mater. Res. A* **2004**, *68*, 383−91.

(15) Rocci, A.; Martignoni, M.; Gottlow, J. *Clin. Implant Dent. Relat. Res.* **2003**, *5* (Suppl 1), 57−63.

(16) Yau, W. W.; Rujitanaroj, P. O.; Lam, L.; Chew, S. Y. *Biomaterials* **2012**, *33*, 2608−28.

(17) Carthew, R. W.; Sontheimer, E. J. *Cell* **2009**, *136*, 642−55.

(18) Chen, J. F.; Mandel, E. M.; Thomson, J. M.; Wu, Q.; Callis, T. E.; Hammond, S. M.; Conlon, F. L.; Wang, D. Z. *Nat. Genet.* **2006**, *38*, 228−33.

(19) Martignani, E.; Miretti, S.; Accornero, P.; Baratta, M. *Mini Rev. Med. Chem.* **2011**, *11*, 1165−82.

(20) Kim, Y. J.; Bae, S. W.; Yu, S. S.; Bae, Y. C.; Jung, J. S. *J. Bone. Miner. Res.* **2009**, *24*, 816−25.

(21) Li, H.; Xie, H.; Liu, W.; Hu, R.; Huang, B.; Tan, Y. F.; Xu, K.; Sheng, Z. F.; Zhou, H. D.; Wu, X. P.; Luo, X. H. *J. Clin. Invest.* **2009**, *119*, 3666−77.

(22) Eskildsen, T.; Taipaleenmaki, H.; Stenvang, J.; Abdallah, B. M.; Ditzel, N.; Nossent, A. Y.; Bak, M.; Kauppinen, S.; Kassem, M. *Proc. Natl. Acad. Sci. USA* **2011**, *108*, 6139−44.

(23) Schoolmeesters, A.; Eklund, T.; Leake, D.; Vermeulen, A.; Smith, Q.; Force Aldred, S.; Fedorov, Y. *PLoS One* **2009**, *4*, e5605.

(24) Li, Z.; Hassan, M. Q.; Jafferji, M.; Aqeilan, R. I.; Garzon, R.; Croce, C. M.; van Wijnen, A. J.; Stein, J. L.; Stein, G. S.; Lian, J. B. *J. Biol. Chem.* **2009**, *284*, 15676−84.

(25) Stenvang, J.; Petri, A.; Lindow, M.; Obad, S.; Kauppinen, S. *Silence* **2012**, *3*, 1.

(26) Wang, Y.; Jiang, X. L.; Yang, S. C.; Lin, X.; He, Y.; Yan, C.; Wu, L.; Chen, G. Q.; Wang, Z. Y.; Wu, Q. *Biomaterials* **2011**, *32*, 9207−17.

(27) Chakravorty, N.; Ivanovski, S.; Prasadam, I.; Crawford, R.; Oloyede, A.; Xiao, Y. *Acta Biomater.* **2012**, *8*, 3516−3523.

(28) Monaghan, M.; Pandit, A. *Adv. Drug Deliv. Rev.* **2011**, *63*, 197−208.

(29) Andersen, M. O.; Howard, K. A.; Paludan, S. R.; Besenbacher, F.; Kjems, J. *Biomaterials* **2008**, *29*, 506−12.

(30) Romoren, K.; Aaberge, A.; Smistad, G.; Thu, B. J.; Evensen, O. *Pharm. Res.* **2004**, *21*, 2340−6.

(31) Teo, B. K.; Goh, S. H.; Kustandi, T. S.; Loh, W. W.; Low, H. Y.; Yim, E. K. *Biomaterials* **2011**, *32*, 9866−75.

(32) Adler, A. F.; Speidel, A. T.; Christoforou, N.; Kolind, K.; Foss, M.; Leong, K. W. *Biomaterials* **2011**, *32*, 3611−9.

(33) Jewell, C. M.; Lynn, D. M. *Curr. Opin. Colloid Interface Sci.* **2008**, *13*, 395−402.

(34) Zhao, L.; Wei, Y.; Li, J.; Han, Y.; Ye, R.; Zhang, Y. *J. Biomed. Mater. Res. A* **2010**, *92*, 432−40.

(35) Cheng, S. T.; Chen, Z. F.; Chen, G. Q. *Biomaterials* **2008**, *29*, 4187−94.

(36) Zhao, L.; Mei, S.; Wang, W.; Chu, P. K.; Wu, Z.; Zhang, Y. *Biomaterials* **2010**, *31*, 2055−2063.

(37) Han, Y.; Chen, D.; Sun, J.; Zhang, Y.; Xu, K. *Acta Biomater.* **2008**, *4*, 1518−29.

(38) Aguiari, P.; Leo, S.; Zavan, B.; Vindigni, V.; Rimessi, A.; Bianchi, K.; Franzin, C.; Cortivo, R.; Rossato, M.; Vettor, R.; Abatangelo, G.; Pozzan, T.; Pinton, P.; Rizzuto, R. *Proc. Natl. Acad. Sci. USA* **2008**, *105*, 1226−31.

(39) Erfle, H.; Neumann, B.; Liebel, U.; Rogers, P.; Held, M.; Walter, T.; Ellenberg, J.; Pepperkok, R. *Nat. Protoc.* **2007**, *2*, 392−9.

(40) Adler, A. F.; Leong, K. W. *Nano Today* **2010**, *5*, 553−569.

(41) Lv, H.; Zhang, S.; Wang, B.; Cui, S.; Yan, J. *J. Controlled Release* **2006**, *114*, 100−9.

(42) Andersen, M. O.; Nygaard, J. V.; Burns, J. S.; Raarup, M. K.; Nyengaard, J. R.; Bunger, C.; Besenbacher, F.; Howard, K. A.; Kassem, M.; Kjems, J. *Mol. Ther.* **2010**, *18*, 2018−27.